Measurement 188 (2022) 110594

Contents lists available at ScienceDirect

Measurement

journal homepage: www.elsevier.com/locate/measurement

Cutting forces and temperature measurements in cryogenic assisted turning of AA2024-T351 alloy: An experimentally validated simulation approach

Munish Kumar Gupta [a,*], Mehmet Erdi Korkmaz [b], Murat Sarıkaya [c], Grzegorz M. Krolczyk [a], Mustafa Günay [b], Szymon Wojciechowski [d]

[a] Faculty of Mechanical Engineering, Opole University of Technology, 76 Proszkowska St., 45-758 Opole, Poland
[b] Department of Mechanical Engineering, Karabük University, Karabük, Turkey
[c] Department of Mechanical Engineering, Sinop University, Sinop, Turkey
[d] Faculty of Mechanical Engineering and Management, Poznan University of Technology, 3 Piotrowo St., 60-965 Poznan, Poland

ARTICLE INFO

Keywords:
Aluminum alloy
Cooling conditions
Cutting forces
Cutting temperature
Machining
Simulation

ABSTRACT

Aluminium alloys are widely used in modern engineering applications such as automobile, aerospace etc because of its characteristics. The machining of aluminium alloys are also considered as difficult because of its sticky and soft nature, low thermal conductivity, strain hardening effect etc. The cooling conditions employed at cutting zone improved the machining performance but the resources, material consumption, skilled labor etc. are also required for performing the machining experiments. Therefore, the simulation of process parameters with the help of Finite Element Modelling (FEM) during machining is highly researched topic these days. In this work, a new practice from measurement science i.e., FEM simulation was performed with AdvantEdge software and the prediction models were developed for evaluating the cutting forces and cutting temperature while machining AA2024-T351 alloy under dry, liquid nitrogen (LN_2) and carbon dioxide (CO_2) conditions. Initially, the 3D turning model was developed and the results were compared with experimental findings. The results obtained from simulation model are very close with experimental results with minimum standard value of 0.67 (5.7%) for cutting forces and 4.58 (6.16%) for cutting temperature. Thus, it is worthy to mention that the 3D FE model is efficient and effective to predict and measurement results with minimum error.

1. Introduction

Aluminum is one of the most used materials in engineering after steel and cast iron [1]. In particular, Al-Cu alloys are increasingly used in aircraft and automotive industries due to its low density (2.7 gm/cm^3), higher strength (18–26 kg/mm^2) compared to other Al alloys, and heat treatment applicability [2,3]. In general, metal materials are not used as much as they are obtained from nature. They have low mechanical properties (hardness, rupture, wear, etc.) as in pure aluminum material. Various methods are applied to improve the mechanical properties of materials. Alloying and heat treatment are some of the applied methods [4]. AA2024-T351 is the addition of alloying elements to pure aluminum material, and then tempering with the process of T351 that means solution heat-treated, stress-relieved with a controlled amount of stretching [5].

In addition to the positive aspects of the changing mechanical properties of the materials, there are also negative aspects. In particular, mechanical properties are directly effective in shaping the material (machining, cutting, bending, etc.) [6]. The shaping of materials by removing chips (turning, milling, drilling, etc.) has an important share in the manufacturing industry [7]. The machinability of the materials is of great importance in terms of cutting tools, cutting forces and surface roughness [8]. In the recent studies, materials were divided into two categories such as easy to machine and difficult to cut materials [9]. The easy and difficult machinability of the material is directly dependent on the mechanical properties of the material (flow, rupture, hardness, etc.) and the cutting parameters. Materials with high mechanical properties (for example, hardness) are difficult to process, while materials with low mechanical properties may be easier to machine. In the processing of materials with high mechanical properties, higher cutting forces and consequently higher temperatures may occur [10]. Although the machining of materials with low mechanical properties seems to be problem-free in terms of cutting forces and cutters, in some materials, it

* Corresponding author.
E-mail addresses: munishguptanit@gmail.com (M.K. Gupta), merdikorkmaz@karabuk.edu.tr (M.E. Korkmaz), msarikaya@sinop.edu.tr (M. Sarıkaya), G.Krolczyk@po.edu.pl (G.M. Krolczyk), mgunay@karabuk.edu.tr (M. Günay), szymon.wojciechowski@put.poznan.pl (S. Wojciechowski).

https://doi.org/10.1016/j.measurement.2021.110594
Received 6 November 2021; Received in revised form 27 November 2021; Accepted 8 December 2021
Available online 13 December 2021

Nomenclature

FEM	Finite Element Modelling
LN_2	liquid nitrogen
CO_2	carbon dioxide
ALE	Arbitrary Lagrangian-Eulerian
BUE	Built-up-Edge
FEA	Finite element analysis
σ^0	flow stress
ε^p	plastic deformation
$\dot{\varepsilon}^p$	deformation rate
$\dot{\varepsilon}_0$	reference plastic deformation rate
T	workpiece temperature
Tm	workpiece melting temperature
Tr	room temperature
A	yield strength (MPa)
B	hardness modulus (MPa)
C	strain rate sensitivity coefficient
n	hardness coefficient
m	thermal softening coefficient
D_1	initial failure strain
D_2	exponential factor
D_3	triaxial factor
D_4	strain rate factor
D_5	temperature factor
V	cutting speed
f	feed rate

can also bring about negativities such as chip adhesion on the cutting insert, deterioration of the surface quality. Especially in the machining of aluminum alloys under dry cutting conditions, negative effects such as deterioration of the machined surface due to Built-up-Edge (BUE) formations and increase in cutting forces are observed a lot [11]. Apart from the mechanical properties of the materials, improperly selected cutting parameters (cutting speed, feed, depth of cut, etc.) can also cause negative effects such as increased cutting forces, low tool life, poor surface roughness [12,13]. For that reason, cryogenic cooling processes are needed to avoid mentioned negativities in machining of aluminum alloys [14,15]. In the cryogenic cooling process, the materials are cooled to very low temperatures (around −196 °C) to achieve the desired metallurgical and microstructural properties [16,17].

Reduction of these temperature is possible by feeding the system with controlled liquid nitrogen (N_2) or CO_2 and using the most suitable insulation materials [18,19]. Some important studies based on cryogenic cooling in machining of various alloys are summarized below. Chetan et al. [20] analyzed the tribological performance of Ti6Al4V alloy in machining with wet and cryogenic cooling conditions. The authors stated that cryogenic cooling is better than wet conditions in machining based on tool wear, carbon emission, machining cost. Ding and Hong [21] studied on cryogenic machining of AISI1008 steel considering, tool wear, temperature and surface quality and found that cryogenic is superior process for better surface quality, less tool temperature and wear. Sivaiah and Chakradhar [22] examined the machinability performance of 17–4 PH stainless steel with coated carbide cutting tools under cryogenic condition. The researchers indicated that cryogenic cooling successfully decrease the cutting region temperature and so can be suggested in machining of difficult to cut materials. Jebaraj et al. [23] compared the coolants of LN_2 and CO_2 in cryogenic machining of AISI L6 steel via TiAlN coated carbide cutting tools. They suggested that CO_2 coolants are better than LN_2 in terms of surface quality while LN_2 conditions are better than CO_2 based on cutting forces. Khanna et al. [24] associated the dry, flood, MQL and cryogenic cooling conditions in machining of stainless steel via carbide inserts. The authors revealed that cryogenic condition is more superior to MQL cooling condition in terms of surface quality, energy consumption and tool wear. Outerio et al. [25] researched on surface integrity in turning of AZ31B-O magnesium alloy under dry and cryogenic cooling conditions and finally showed that cryogenic cooling is better than dry condition based on cutting forces. Kaynak [26] evaluated the machinability performance of Inconel718 alloy under dry, MQL and cryogenic cooling conditions. The scientist conclusively found that cryogenic is the best machining condition based on tool wear and cutting zone temperature, while MQL is the best condition on surface quality. Eapen et al. [27] studied on dry and cryogenic machining of AA6063 aluminum alloy and dedicated that cryogenic condition is more suitable than dry condition for higher surface quality.

As mentioned above, these studies are commonly costly, material wasting and thus not eco-friendly. Therefore, some numerical methods are suggested in the research field. The most used in machining processes are the finite element method. Finite element (FE) method, providing the resolution of a complicated problem, is a popular and effective method used in several engineering applications [28]. Complex engineering problems involve complex solutions. This confusion also distracts the solution phase from sensitivity. The finite element method can be used to solve complex problems in the shortest way with the closest solution to the right result. The main finite element software's used in the machining industry are DEFORM 3D, LS-Dyna, ABAQUS and Thirdwave Advantedge. Several critical studies based on FE in machining of aluminum alloys are summarized below. Li et al. [29] verified the finite element model of experimental high speed machining process with AA6061-T6 aluminum alloy. The authors also confirmed the Johnson-Cook model parameters of this alloy that are previously determined experimentally under high strain rates. Mali et al. [30] validated the simulational cutting forces with the experimental results by performing dry turning process to AA7075 aluminum alloys. The researchers also compared and confirmed the tool wear, chip behaviour and stresses on the cutting inserts from FE model. Lima et al. [31] studied on comparison of cutting temperatures between FE and experimental results in milling of AISI D2 steel by thermocouple methods and the finally verified the FE model by experimental conditions. Baraheni et al. [32] developed a FE model for ultrasonic drilling of 7075 aluminum alloy. The researchers verified the FE model through experimental drilling tests by higher than 80% accuracy. Khajehzadeh et al. [33] compared the experimental and FE results of ultrasonic turning for AISI 4140 steel. The scientists verified the FE thrust forces and residual stress via experimental drilling tests by 91% and 87%, respectively. Huang et al. [34] created a FE model for high speed milling of aluminum 7075 alloy and then confirmed the model with experimental milling processes under same conditions by high accuracy.

It is seen that studies of FE machining based on cryogenic cooling conditions for AA2024-T351 alloy is very limited in the literature. Although this alloy is highly used in aerospace applications, but still the work on simulation under different cooling condition is quiet limited. Therefore, the purpose of this research is to develop a FE model based on dry and LN_2/CO_2 cryogenic turning, and evaluate the performance of machinability in terms of cutting forces and cutting temperature for AA2024-T351 alloy. Moreover, the main aim is to contribute to the solution of the important problems mentioned in the related research on manufacturing. It is observed that there are differences in the cooling techniques used in scientific research and manufacturing. In this regard, it is intended that the results of this study are directly engaged in manufacturing and scientific research. Initially, the 3D cryogenic model was developed with FEM practice and the responses were predicted. Then, the comparison has been made with experimental results. The

complete analysis of this work is shown in next sections.

2. Formulation of 3D cryogenic assisted Johnson-Cook turning model

2.1. Introduction of FE model

One of the most widely used solutions in recent years is finite element analysis, which divides complicated systems into particles, transforms them into idealized structures, and solves them mathematically [35]. For derivatives of finite elements, which are subcomponents of approximation functions, the finite element approach follows specific procedures [36]. The numerical solution procedure for parameters at specific points is defined as the nodes of each element and is applied to the computation of finite solutions when determining the solution to the problem for the entire geometry [37]. Finite element analysis (FEA) is considered as an effective method that can be used to solve problems that are difficult or impossible to solve analytically [38]. The initial stage in finite element analysis is to discretize the geometry, after which the geometry is split into finite elements. The Arbitrary Lagrangian-Eulerian (ALE) mesh does not fix points on the geometry surface to the material or to a specific region; instead, it is based on arbitrary movement of points and that's why, the material flow is point-independent. Compared to both mesh topologies, ALE produces better outcomes [39]. ALE network algorithms are used in more than one software to solve metal cutting problems. Some of them are ABAQUS, DEFORM, Third Wave AdvantEdge, ANSYS LS-DYNA, and from them, users get very good results. The re-meshing technique employed in several software's helps further reduce errors in the analysis [40]. Tetrahedral meshes used in this FE study are utilized in a variety of applications, including fracture, haptics, solid modeling, surgical simulations, and the modeling of biological tissue such as the brain, knee, and even adipose tissue, as well as machining simulations. In order to analyze chip formation using the finite element method in machining operations, some boundary conditions need to be defined [41]. The entered boundary conditions play an active role in defining the limits and loading conditions to solve the problem. It is feasible to simulate chip formation by selecting the right modeling approach, establishing the boundary conditions, calculating the material's deformation rate, and knowing how the workpiece material will react during plastic deformation [42]. The strain rate and heat effects of the constitutive equations must be set to define the model's dynamic behavior [43]. In metallic materials, stress, strain and strain rate vary with temperature [44]. One of the most important models considering strain and heat effects in metallic materials is the Johnson-Cook (JC) constitutive model [45]. Moreover, it is possible to create material models such as rigid plastic, elastic–plastic, thermo-elastoplastic, thermo visco-plastic by using these models [46]. The Johnson-Cook constitutive model employed [47] by Third Wave AdvantEdge can be seen in Eq. (1).

$$\sigma^0 = (A + B(\varepsilon^p)^n)\left(1 + Cln\left(\frac{\dot{\varepsilon}^p}{\dot{\varepsilon}_0}\right)\right)\left(1 - \left(\frac{T - T_r}{T_m - T_r}\right)^m\right) \quad (1)$$

In Eq. (1), σ^0, ε^p, $\dot{\varepsilon}^p$, $\dot{\varepsilon}_0$, *T, Tm and Tr* represent flow stress, plastic deformation, deformation rate, refers to reference plastic deformation rate, workpiece temperature, workpiece melting temperature, room temperature, respectively. The coefficient *A, B, C, n, and m* show yield strength in MPa, hardness modulus in MPa, strain rate sensitivity coefficient, hardness coefficient and thermal softening coefficient, respectively [47]. Also, a damage model is needed for chip separation. For equivalent fracture strain, JC damage model [48] is used as seen in Eq. (2).

$$\overline{\varepsilon}^f = \left(D_1 + D_2\exp(D_3\frac{P}{\overline{\sigma}})\right)\left(1 + D_4 ln\left(\frac{\dot{\overline{\varepsilon}}}{\dot{\overline{\varepsilon}}_0}\right)\right)\left(1 + D_5\left(\frac{T - T_r}{T_m - T_r}\right)\right) \quad (2)$$

Here, stress triaxiality is represented by $\frac{P}{\overline{\sigma}}$ and P refers to hydrostatic pressure which is the mean of three-dimensional normal stresses. $\overline{\varepsilon}^f$ denotes the fracture strain experienced at chip separation that is a part of dynamic metal cutting processes. In addition, D_1, D_2, D_3, D_4 and D_5 are constants for initial failure strain, exponential factor, triaxial factor, strain rate factor and temperature factor, respectively. The general geometric structure for finite element analysis with Third Wave AdvantEdge is presented in Fig. 1. As the turning method, 3D nose turning shown was preferred. Fig. 1 shows the overall geometric framework for finite element analysis through by with Third Wave AdvantEdge. The 3D nose turning approach was chosen in cutting process.

2.2. Work piece and cooling condition details

The appropriate transfer of the material model to the software is critical to the success of the numerical analysis of machining. For this reason, the correct determination of material properties and adapting them as inputs reflect the success of the modeling. In present study, AA2204-T351 workpiece material with dimensions of 1x1x3 mm was used for the finite element analysis. The JC parameters in Table 1, fracture constants in Table 2, chemical composition in Table 3 and mechanical and thermal features of AA2204-T351 alloy in Table 4 can be seen.

As illustrated in Fig. 2, the cutting tool was CVD coated TiC-Al2O3-TiN carbide insert (each presumed to be 1 m thickness [50]) with an ISO number of CNMG 120408. Table 5 lists the characteristics of utilized carbide cutting insert.

Cryogenic basically refers to very low temperatures [52]. Although several assumptions exist, the temperature that separates cryogenic from ordinary cryogen is usually regarded as −150° C. Based on this assumption, cryogens with a boiling temperature above −150 °C, which are used in local cooling such as air conditioning and freezers, are classified as conventional coolers, whereas cryogens with a boiling temperature below −150 °C, such as hydrogen, CO_2, and LN_2, are classified as non-conventional coolers. When studying a system that operates at cryogenic temperatures, it's important to remember that materials' thermal characteristics fluctuate with temperature. For heat transfer calculations at cryogenic temperatures, specific heat, thermal conductivity, and notably heat transfer coefficient values for gases and liquids are significant thermal characteristics. Eq. (3) gives the formula for calculating heat transfer per unit time (*Q*) [53].

$$Q = C_v * m * \frac{dT}{dt} \quad (3)$$

Here, *Cv, m* and *dT/dt* show the specific heat, the mass and the rate of

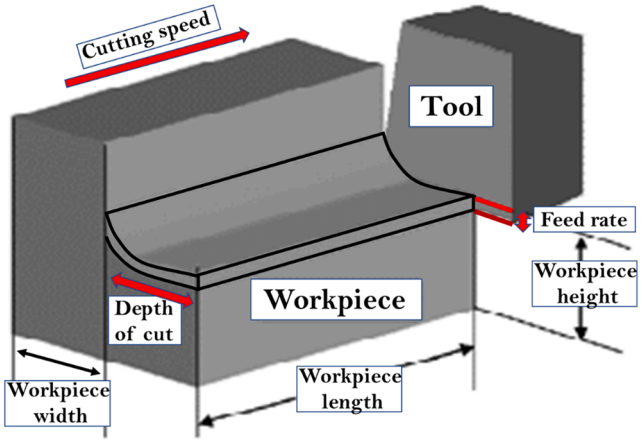

Fig. 1. The overall geometric framework of finite element analysis.

Table 1
JC parameters of AA2204-T351 alloy [49].

A (MPa)	B (MPa)	n	C	m
352	440	0.42	0.0083	1

Table 2
JC fracture constants of AA2204-T351 alloy [49].

D1	D2	D3	D4	D5
0.13	0.13	1.5	0.011	0

Table 3
The chemical content of AA2204-T351 alloys [49].

Cu	Mg	Mn	Si	Fe	Zn	Cr	Ti	Al
4.9	1.2–1.8	0.3–0.9	0.5	0.5	0.25	0.1	0.15	Bal

Table 4
The other mechanical and thermal properties of AA2204-T351 alloy [49].

E (GPa)	T_m (°C)	α (10^{-6}/°C)	k (W/mK)	υ	ρ (kg/m^3)	c_p (J/kg°C)
73	520	8.9	114.4	0.33	2700	877.6

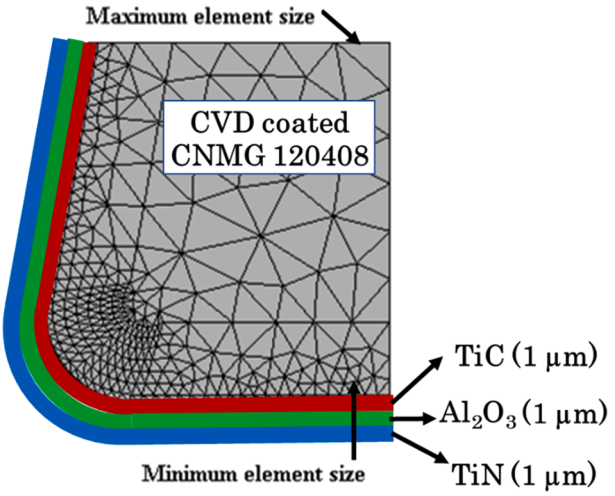

Fig. 2. Input of cutting tool parameters to the system.

Table 5
The mechanical and thermal properties of the carbide insert [51]

E (GPa)	k (W/mK)	α (10^{-6}/°C)	υ	ρ (kg/m^3)	c_p (J/kg°C)
640	50	4.5	0.22	11,900	220

temperature decrease per unit time, respectively. By substituting "$m = A^*\delta^*\rho$" in Eq. (4);

$$Q = C_v{}^*A^*\delta^*\rho^*\frac{dT}{dt} \tag{4}$$

The heat flux density "q" can be obtained from "Q/A". Therefore, as a result of Newton's heat transfer rules, Eq. (3) takes the form of Eq. (5).

$$q = \rho^*C_v{}^*\delta^*\frac{dT}{dt} \tag{5}$$

Here, dT/dt is the ratio of the temperature differences such as the cooling rate *(T2-T1)/(t2-t1)*.

$$h = \frac{q}{T_w - T_f} \tag{6}$$

In Eq. (6), "h" represents the heat transfer coefficient in W/m^2K *and* T_w and T_f indicate the surface temperature and cryogen temperature of LN_2 (−196.5 °C) and CO_2 (−78.5 °C), respectively. In addition, as illustrated in Fig. 3, the heat transfer coefficients for LN_2 and CO_2 were inputted as 309 W/m^2K and 165 W/m^2K [54].

2.3. Meshing details

The mesh structure used in finite element analysis has a big impact on the final findings [51]. The basic objective is to create a mesh structure that can accurately reflect the geometry. The density of FEs is an important metric for determining the correctness of a study. In addition, the accuracy of the analysis is also influenced by the element type and morphology. Assuming there is no singularity area in the model, the greater density mesh gives highly precise results. The model's element mesh, however, is extremely thick, necessitating a large amount of computer memory and a lengthy execution time. The issue is especially prevalent in nonlinear and transitional analysis when many recurring circumstances are present. One method of evaluating the quality of a finite element mesh is to compare the results to test data or theoretical values. However, test data and theoretical findings are typically unavailable in the early phases of research. As a result, new tools for evaluating mesh quality are necessary. Meshing sensitivity analysis is the most significant of them. In this paper, mesh susceptibility analysis using the re-meshing approach provided in Table 6 was used to reduce the minimum element size for the workpiece and cutting tool to 0.15 mm. The software was run on a machine with 16 GB of RAM, 6 GB of client cache, and a CPU speed of 2.4 GHz. To solve FE analysis quicker, all 8 cores of the computer were employed for parallel processing. First, the element sizes of 1, 0.5, and 0.25 mm were utilized in the FE analysis, and the results were 105.7, 95.9, and 87.2 N, respectively, with computation times of 0.6, 1.3, and 3.8 h. Because of the greater values of change in cutting forces in tiny computing time differences, the element size should be reduced. Afterthat, the element size was gradually reduced to 0.1 mm. Although the difference in cutting force is negligible, the calculation time was increased by approx. 84%. As a result, the element size was set to 0.15 mm for a basic test simulation with a computing time of 6.1 h, as shown in Table 6.

2.4. Friction model details

The Coulomb friction model can provide accurate results on the tool flank face in FE simulations of the turning process. [55]. In present investigation of orthogonal turning, the average friction coefficient (μ) between tool and chip was assumed as 0.45. Fig. 4 depicts the standard

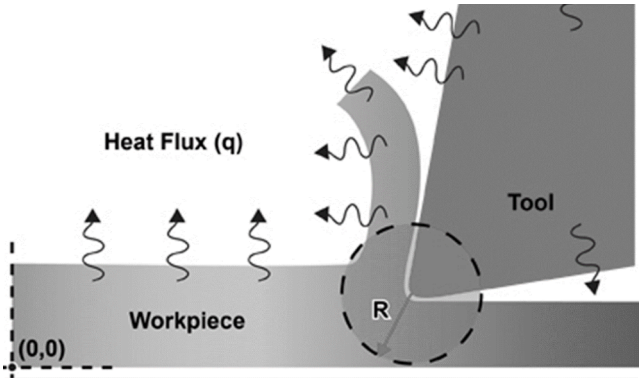

Fig. 3. Coolant inputs for LN_2 and CO_2 cryogens.

Table 6
The mesh sensitivity analysis for a simple analysis

Element size (mm)	Cutting force (N)	Simulation solving time (h)
1	105.7	0.6
0.5	95.9	1.3
0.25	87.2	3.8
0.2	82.4	5.1
0.15	**79.5**	**6.1**
0.1	79.1	11.2

flow chart for FEs.

3. Results and discussions

In this simulation study, the 3D turning was analyzed and a new finite element model was developed with Thirdwave Advantage software using the process parameters and boundary conditions detailed above. The detail of simulation results are given below:

3.1. Analysis of predicted cutting forces

Determination of cutting forces are very important for machine tool design and cutting parameters, workpiece material, cutting tool properties and cutting environment are the most basic factors that significantly effectss the cutting force values [56]. Moreover, the cutting forces are very helpful in estimating cutting power, surface roughness and tool wear values. Therefore, the minimum cutting forces are required in all machining operations to obtain the sound machining characteristics. The finite element analysis results of cutting forces and its influence are presented graphically in Fig. 5. In general, FEM-obtained cutting force variations tended to be similar for all cutting media and increased with increasing feed rate. This result can be associated with the increase in the contact area at the tool-chip interface with the increase in feed rate and the removal of more material per unit time, as can be stated in Refs. [57,58]. It is also thought that increasing friction in the feed direction with increasing feed rate [59] is also thought to contribute to the increase in cutting forces. However, the lower cutting forces in LN_2 and CO_2 cutting environments can be explained by the decrease in the negative effects of friction in the second deformation zone. Thanks to the cooling and lubricating effect of LN_2 and CO_2 gases, the minimum BUE and sticking zone have resulted in lower cutting forces. On the other hand, contrary to expectations, cutting forces increased with increasing cutting speed in FEM simulations. This can be explained by the metallurgical changes that occur with the thermo-mechanical effect during the deformation of the material. In general, the increased heat during deformation can cause strain hardening as well as a softening effect in the workpiece. In another sense, the strain hardening effect exceeds the softening effect when there is not a high enough shear rate to cause thermal softening. In this case, there is an increase in material strength and, as a result, an increase in shear forces. A similar observation was also done by Hou et al. [60] and Shi et al. [61]. Moreover, Paresi et al. [62] proved that the strength of AA2024-T351 material increased due to strain hardening up to 200 °C at high deformation rate. From Fig. 5, it has been seen that the minimum cutting forces are determined under LN_2 cooling followed by CO_2 and dry environment. The liquid nitrogen cooling reduces the forces upto 5.05% and carbon dioxide reduces the forces upto 1.58% as compared with dry machining. This may be attributed to the fact that the low cutting temperature under liquid nitrogen cooling condition results the improvement of strength of cutting tool hardness with lower values of tool wear and as a result, less adhesion is occured between tool and chip interface [63]. Another fact, the liquid nitrogen boiling temperature is significanlty less than carbon dioxide and this low boiling temperature prevents the workpiece and tool material from overheating [64]. The other reason is that the liquid nitrogen absorbs the heat very quickly and provides good lubrication effect at cutting zone [65].

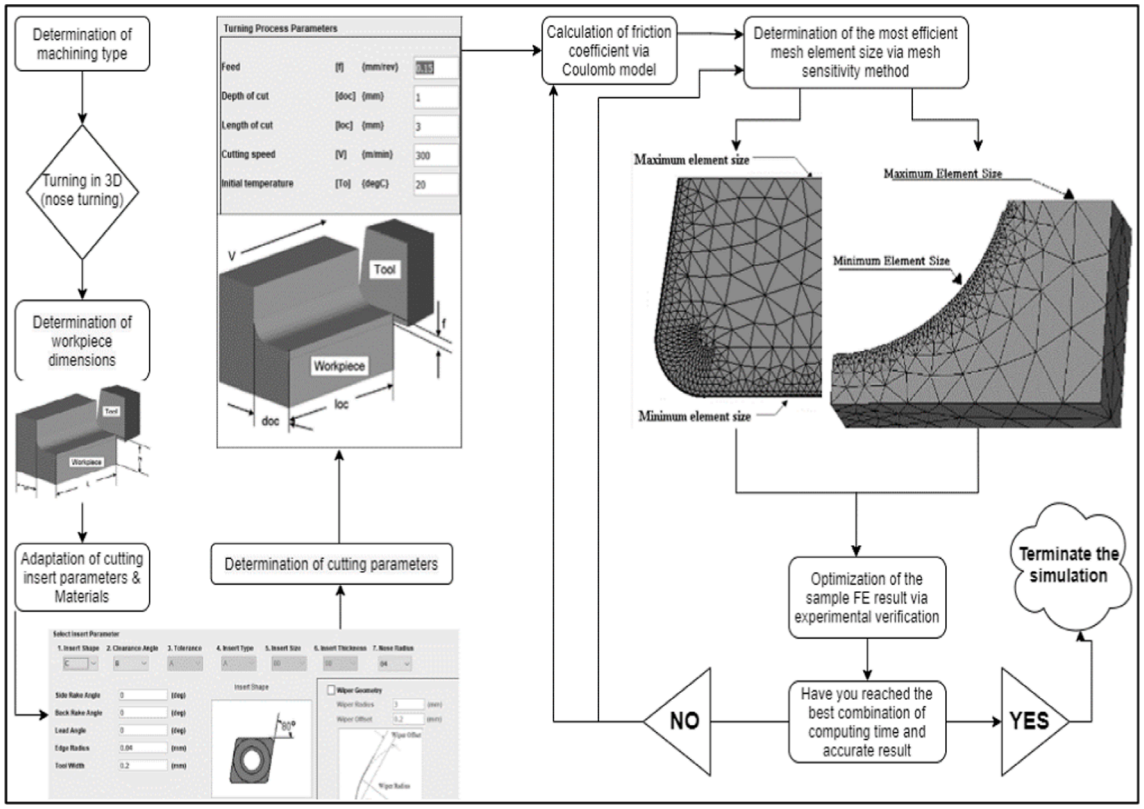

Fig. 4. The flow chart of the FE simulations.

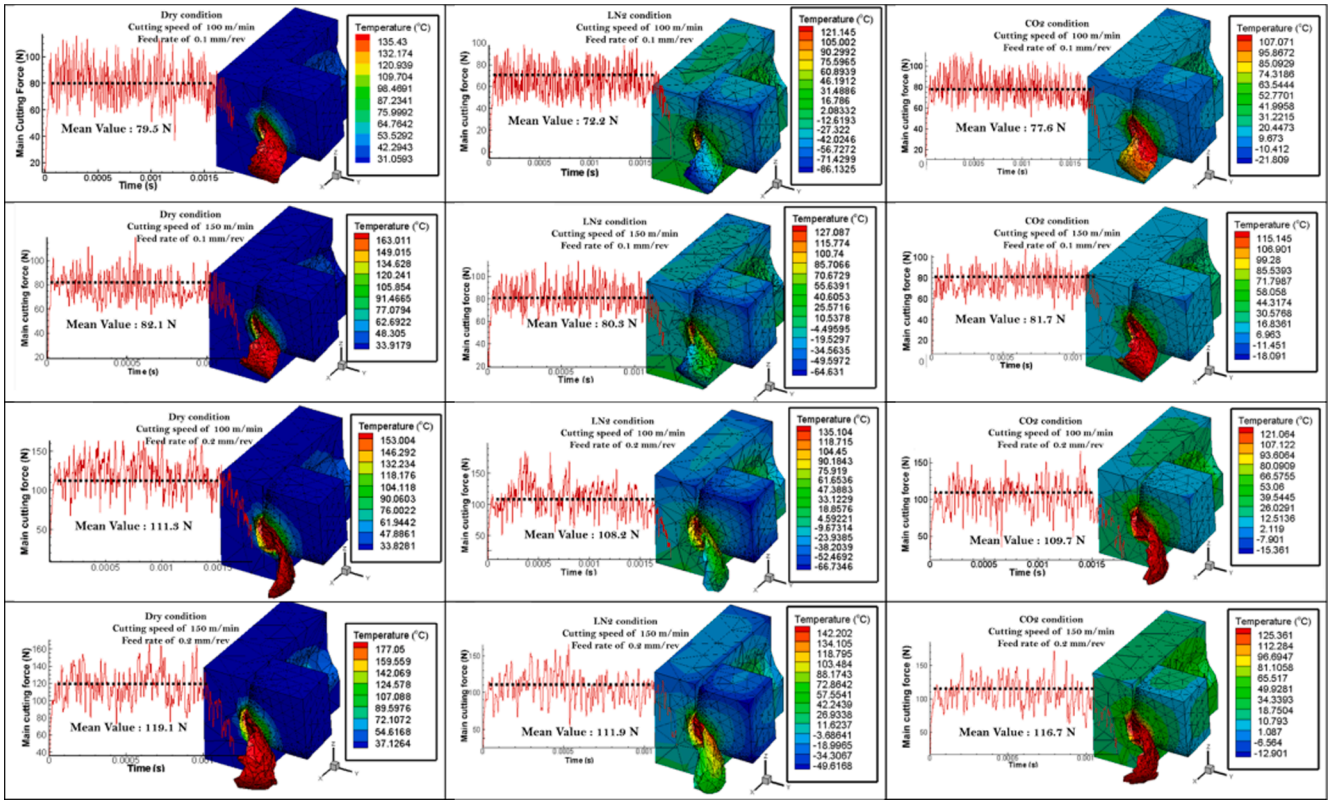

Fig. 5. FE results of Dry, LN_2, and CO_2 condition.

3.2. Analysis of predicted cutting temperature

In order to examine the machining performance, it's very important to determine the temperature especially at the cutting zone during machining operation. The aluminium is as soft as titanium alloy having low thermal conductivity [66] this property of aluminium alloy results in higher cutting temperature at cutting zone. The poor thermal conductivity of the Al alloy like titanium alloys means that only 20% of the heat generated is removed from the machining area [67]. Fig. 5 also demonstrates the FEM results of cutting temperature while machining aluminium alloy under different cooling conditions. During the machining of soft materials like aluminium alloys, the heat is not evacuated from cutting zone and as a results, the build up edge accelerates with the increase in cutting speed values [68]. Similarly, the feed rate is also noticed at dominant factor effect the cutting temperature values and when the feed rate is increased, the value of cutting temperature is also increased upto 10%, respectively. This can be attributed to the greater feed, which increases the cutting temperature by promoting energy in the system and producing more friction between the machined workpiece material and the cutting insert. This result supports the literature [69,70]. On the other side, the cutting temperature values are less in the case of carbon dioxide cooling and this is due to the fact that when CO_2 is transferred to the tool-chip contact area, cryogenic liquid absorbs heat and dissipates quickly from the region, which is the main factor in further lowering the cutting temperature. Therefore, the drop of temperature under CO_2 has been noticed from 11% and 26% respectively as compared with LN_2 and dry environment. This is also evidence that the cooling efficiency of CO_2 decreases at elevated cutting speeds and feed rates. Moreover, the application of both cryogenic cooling conditions help to break the chips into small pieces. With this phenomena, the rubbing of chips with cutting tool is reduced and as a result, less friction was generated at tool-chip interface as mentioned by Danish et al. [71]. Hence, the temperature has been reduced as compared with dry machining. The complete mechanism of chip breakage is also shown in Fig. 6.

3.3. Verification of FE by turning experiments

3.3.1. Experimental procedure for verification

The simulation was carried out under the same experimental test conditions. Machining of commercially available AA2024-T351 alloy was carried out using CVD TiCn-Al_2O_3-TiN coated carbide cutting tools with ISO designation of CNMG 120408. The workpiece had a diameter of 30 mm and a length of 100 mm. To reduce the effect of work hardening, the first 0.5 mm layer was removed. The 0.8 mm nose radius, the side cutting edge angle, also known as principal cutting angle, was 90° in this study. Moreover, the actual tests were also carried out at same conditions with FE simulations. The CNC lathe machine was utilized for this aim. Table 7 lists the machine tool as well as the cryogenic cooling system characteristics. The process parameter levels were chosen using a tool manufacturer's handbook and preliminary tests. The experimental design is shown in Annexure 1. During the experiments, a depth of cut of 0.5 mm was used and a machining time of 60 s was taken into account. Table 8 lists the cutting parameters in detail. Then, using a Fluke thermal camera and a Kistler 9257A dynamometer, the cutting temperature and cutting forces were measured. The positioning of the thermal camera was on rake face from which the temperature from main cutting zone or primary share zone was measured. Moreover, during the temperature measurements with thermal camera, the main problem is (usually) the measurement of temperature onto the outer plane of flowing chip, whereas in FEM model the direct temperature in the cutting zone is evaluated. Thus, it is difficult to compare the temperatures measured on the distinct zones. However, to solve this problem, initially the temperature were measured and calibrated with simulation results and the overall, cutting temperature values during the machining experiments were considered for comparison. All measurements were taken five times and after that the average values were considered for analysis. Mentioned measurements were performed online and

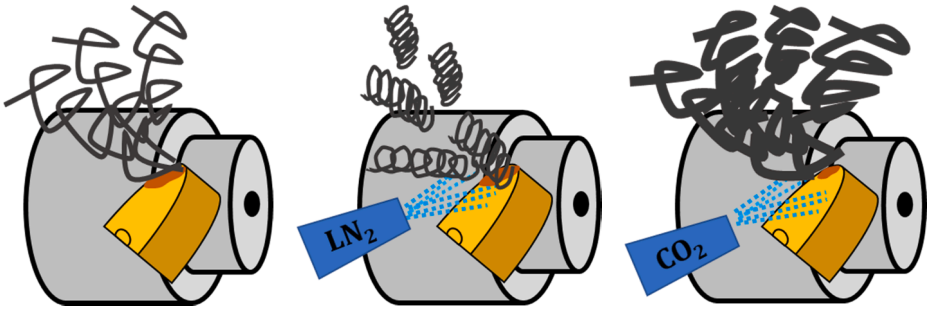

Fig. 6. Chip mechanism under different cooling conditions (a) Long and continuous chips, (b) & (c) Short chips due to cryogenic cooling.

Table 7
Technical parameters of CNC turning center and cooling conditions

Machine	Specifications
CNC lathe machine	Minimum and maximum spindle speed 200–3000 RPM with 6KW motor.
Cooling condition details	Flow rate of coolant: 0.35 L/min, pressure: 4 bar, dimensions of nozzle: 1 mm brass nozzle diameter, 2 nozzles with position at rake face

Table 8
The machining factors and their levels

Factors	Level		
	1	2	3
Cutting speed (V)	100	–	150
Feed rate (f)	0.1	–	0.2
Cooling conditions	Dry	LN_2	CO_2

Dynoware software was used to transfer the cutting forces information to computer. Fig. 7 depicts the study's overall flow diagram.

3.3.2. Analysis of results

The experimental, simulation and deviation results are shown in Figs. 8 and 9. It is seen from Fig. 8 (a)–(c) that the Fc values obtained with FEM are relatively larger than the experimental data when the feed rate is 0.2 mm/rev. This result can be explained by the pressure formed in the second deformation zone as the feed increases. The segmented chip formation [49] increases with the increase in feed and it also increases the pressure created by the friction effect at the tool-chip interface, thus increasing the cutting forces. When the experimental and numerical analysis results are examined, it has been determined that the cutting media that offers the lowest cutting forces is LN_2 cooling, followed by CO_2 and dry environment. The lowest cutting force was found in 0.1 mm/rev feed, 100 m/min cutting speed and LN_2 cutting environment. Compared to dry cutting, an average of 8.8% less cutting force was obtained in LN_2 assisted machining and 4.4% less in CO_2 assisted machining. In addition, the experiment run # 4 i.e., cutting speed of 150 m/min, feed rate of 0.20 mm/rev and dry conditions shown in Fig. 8 (c) provides the minimum standard deviation value of 0.67 and the average deviation value obtained were 5.71. Therefore, it is worthy to mention that the simulation model developed for cutting forces are

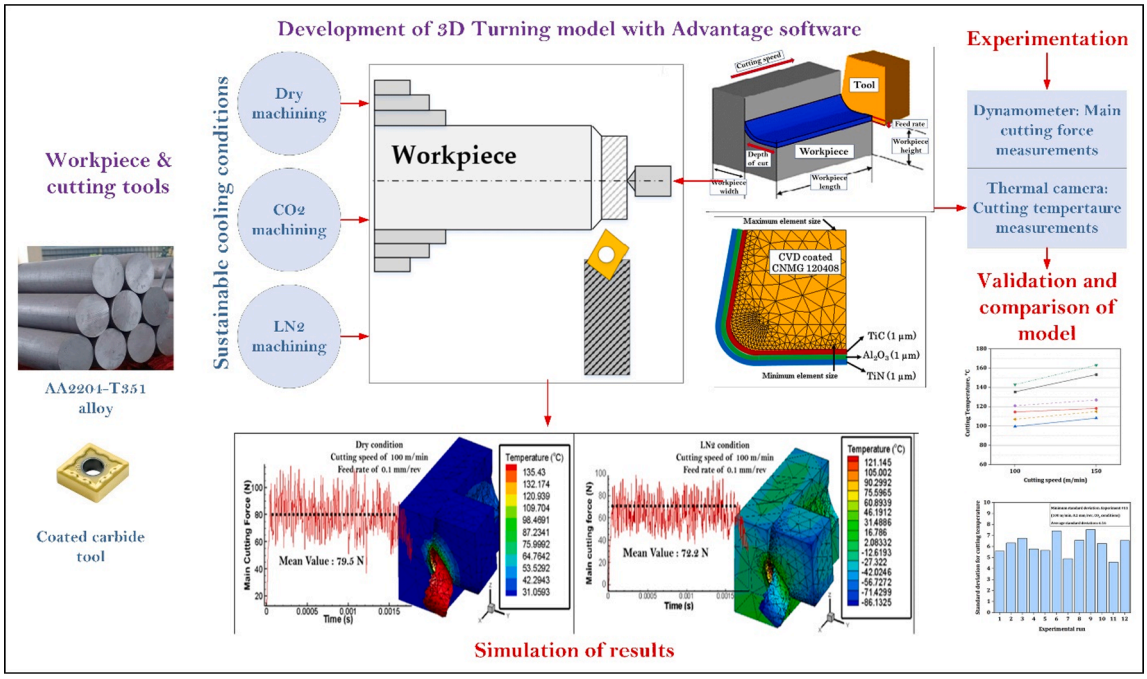

Fig. 7. The general flow chart of the study.

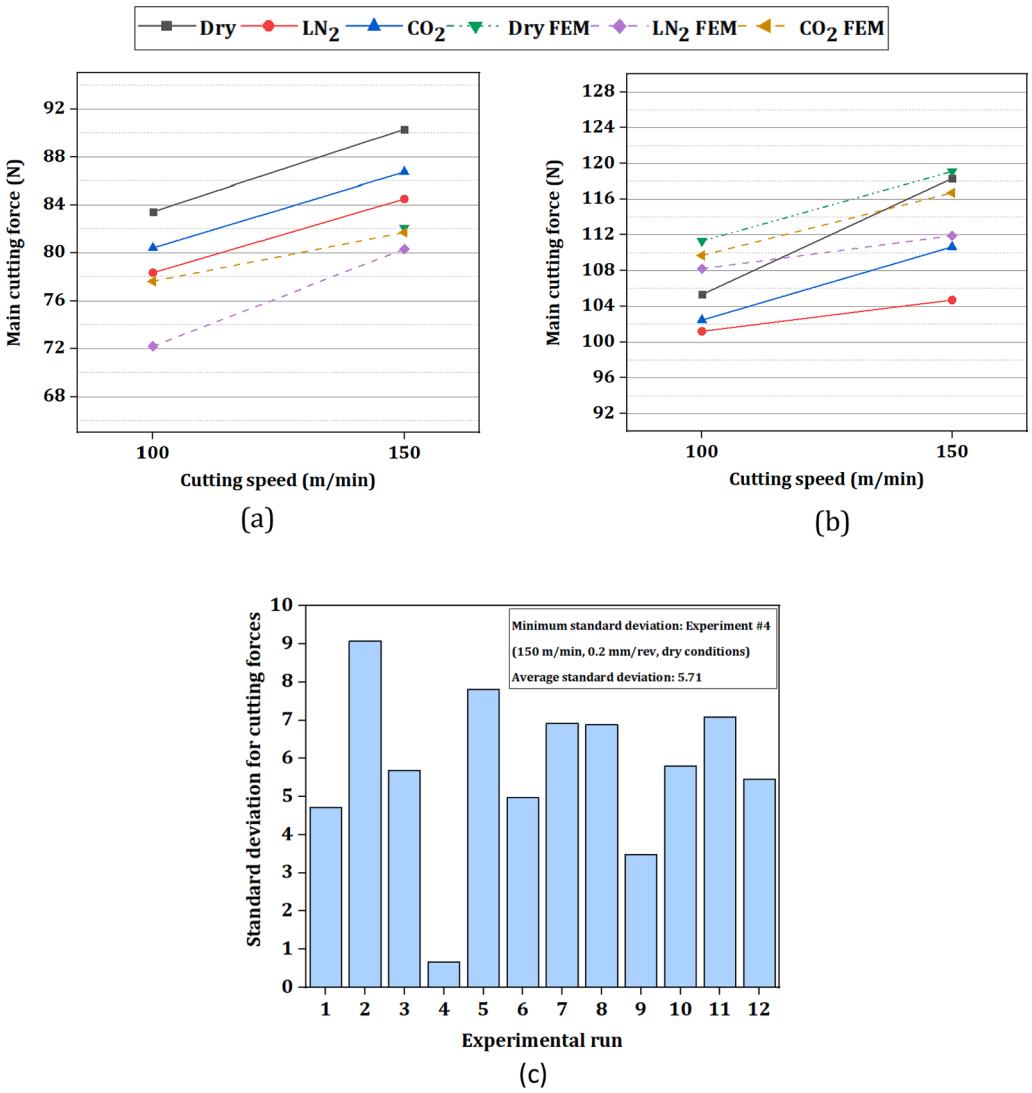

Fig. 8. Comparison of main cutting force; a) f = 0.1 mm/rev, b) f = 0.2 mm/rev and (c) Deviation of cutting forces results with respect to experimental results.

very close to experimental values, respectively. Hence, the developed model is suitable for prediction of cutting forces under specified cutting conditions.

Similarly, the experimental, simulation and standard deviation values of cutting temperature are shown in Fig. 9 (a)–(c), respectively. It can be seen that the cutting temperatures obtained in experimental and FEM simulation remain within the temperature threshold mentioned in the literature (Fig. 9). When this situation is compared with respect to cutting media, the highest increase in cutting temperature with increasing cutting speed is 22 °C in dry cutting, while it is around 5 °C in LN_2 and CO_2 cutting environments. When the cutting temperatures are compared, experimentally and numerically the smallest temperature value was obtained in the CO_2 environment at the smallest feed and cutting speed. In the light of all the evaluations, the average 5.7% and 6.16% deviations between the experimental and cutting simulations, respectively, in terms of cutting force and cutting temperature indicate the suitability of the JC material model, coefficient of friction and FEM simulations. In the literature, most of the FE machining studies shows that the deviation less than about 10% is thought as the acceptable range between the finite element model results and experimental validation [72,73]. In addition, the experiment run # 11 i.e., cutting speed of 100 m/min, feed rate of 0.20 mm/rev and CO_2 cooling conditions shown in Fig. 9 (c) provides the minimum standard deviation value of 4.58 and the average deviation value obtained were 6.16, respectively. Therefore, it is worthy to mention that the simulation model developed for cutting temperature is very close to experimental values. Hence, the developed model is suitable for prediction of cutting temperature under specified cutting conditions.

3.3.3. *Discussion and comparison of the results*

During comparison of FEM and experimental results, the development of friction model and meshing accuracy plays an important role. Apart from these, the selection of Johnson Cook parameters that specifically matches the material properties is highly important to get the accurate results. The mechanical features, microstructure, and other characteristics of the workpiece material employed in this study, however, may differ from those reported in the literature for the same material [74]. The strength of the interatomic connection is primarily responsible for mechanical qualities. Furthermore, the material's microstructure has an major impact and different mechanical properties such as tensile strength, compressive strength, hardness, and toughness of the same material can be achieved by modifying the microstructure [75]. In addition, the same material have different tensile strength values and thats why, researchers considered the average of 4–5 tensile strength values from the same test situation [76,77]. Moreover, the precipitation hardening properties of material plays an active role to differentiate the texture of same materials. The strength of the material is increased because the material is separated from the main phase in the

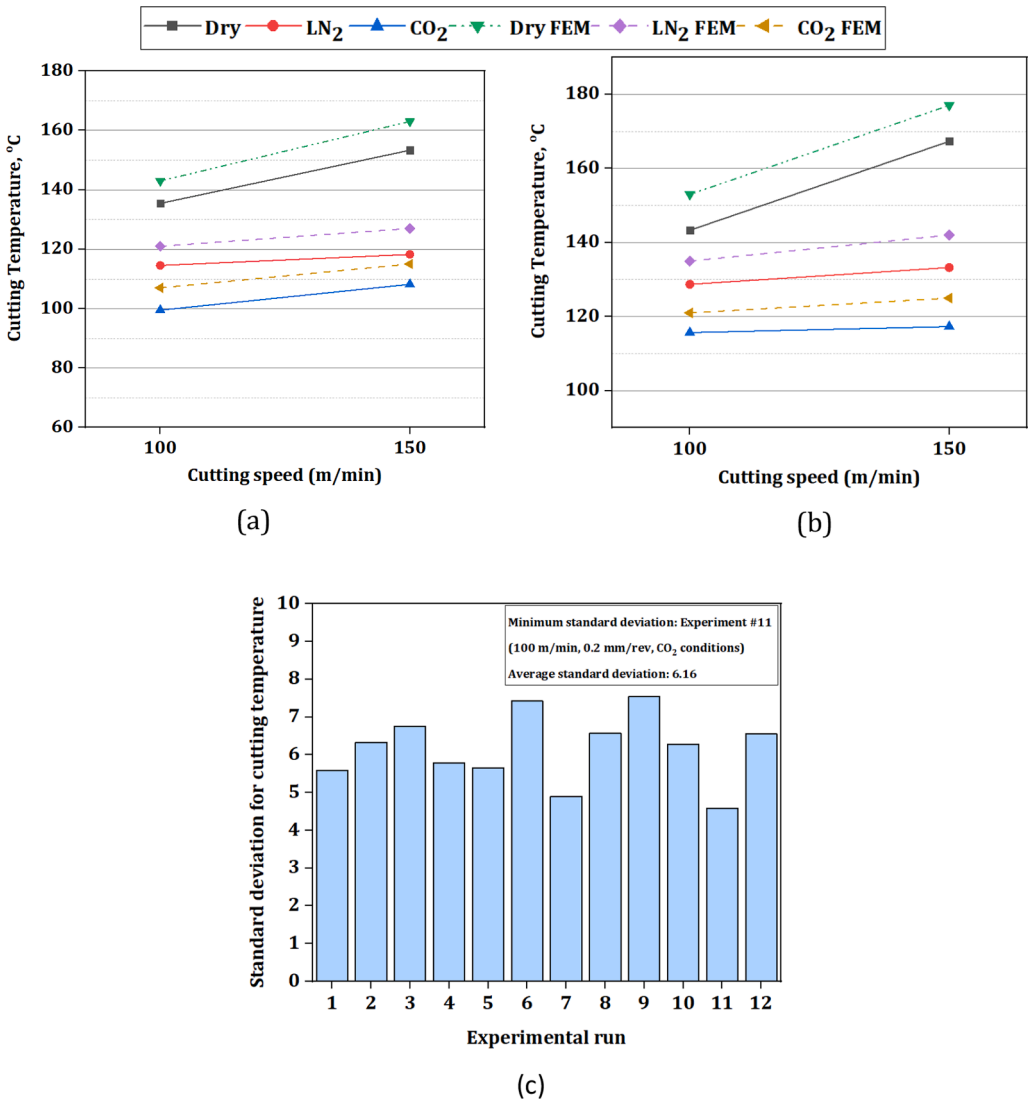

Fig. 9. Comparison of cutting temperature; a) f = 0.1 mm/rev, b) f = 0.2 mm/rev (c) Deviation of cutting temperature results with respect to experimental results.

form of particles [78]. This process is mostly used to increase the strength of material generally in the case of non ferrous materails such as Ti, Al, Mg [79]. The prevention of the displacement movement of the precipitates created by the precipitation of supersaturated melts is the major explanation for the enhanced strength with precipitation hardening. However, the compatible material in the finite element software can behave in the same way as certain compatible parameters, such as JC inputs, constants, tensile parameters, Young's modulus, and so on. No special conditions can be defined for the structure of the material in the certain software. Therefore, a mean deviation of 5–6% can be due to these situations. It was emphasized by [80] that the reason for the deviation can be caused by less accurate engagement and friction models. In addition, similar findings were also reported by Korkmaz et al. [47]. The researchers have attributed the inconsistency to both the structure and hardness of the workpiece material. It is also among the reasons that the depth of cut is less than the radius of the cutting edge. Thats why, FE software cannot model this effect and under cryogenic conditions, the heat transfer coefficient is assumed to be constant. Since, the cutting and cooling process is a thermodynamic process, therefore it really needs to be modeled dynamically [81] or as a function of temperature [82]. However, solving a simple FE simulation under cryogenic conditions can be very time consuming and thats why the heat transfer coefficients are kept to be constant.

4. Conclusions

The study aims on the AA2204-T351 turning process under LN_2/CO_2 cooling and uses FEM to model this process. The purpose of this study is to analyze the extent to which the widely adopted LN_2/CO_2 cooling technology performs its intended function to meet the requirements for sustainable processing. In addition, in light of the FEM data of this study, it aims to validate the FEM simulation study through an experimental turning process and to validate the evaluation of the results obtainable from the machining process. The main results of this study can be summarized as follows.

- Liquid nitrogen cooling lowers the cutting forces upto 5.05% and carbon dioxide cooling reduces the cutting forces upto 1.58% as compared with dry conditions.
- When CO_2 is injected to the tool-chip contact region, it absorbs heat and evaporates rapidly from area, causing the cutting temperature to drop. CO_2 has the lowest cutting temperature than LN_2 and dry environment by 11% and 26%, respectively. This is evidence that the cooling efficiency of CO_2 decreases at elevated cutting speeds and feed rates.
- The lowest cutting force was found at 0.1 mm/rev feed, 100 m/min cutting speed and LN_2 cutting environment. Compared to dry

cutting, an average of 8.8% less cutting force was obtained in LN_2 assisted machining and 4.4% less in CO_2 assisted machining.

- The highest increase in cutting temperature with increasing cutting speed is 22 °C in dry cutting, while it is around 5 °C in LN_2 and CO_2 cutting environments. When the cutting temperatures are compared, experimentally and numerically the smallest temperature value was obtained in the CO_2 environment at the smallest feed and cutting speed.
- In the light of all the evaluations, the average of 5.7% and 6.16% deviations between the experimental and cutting simulations were observed and the results indicate the suitability of the JC material model, coefficient of friction and FEM simulations.

CRediT authorship contribution statement

Munish Kumar Gupta: Investigation, Formal analysis, Conceptualization, Writing – review & editing. **Mehmet Erdi Korkmaz:** Investigation, Formal analysis, Conceptualization, Writing – review & editing. **Murat Sarıkaya:** Investigation, Formal analysis, Conceptualization, Writing – review & editing. **Grzegorz M. Krolczyk:** Conceptualization, Writing – review & editing, Supervision. **Mustafa Günay:** Conceptualization, Writing – review & editing, Supervision. **Szymon Wojciechowski:** Conceptualization, Writing – review & editing, Supervision.

Declaration of Competing Interest

The authors declare that they have no known competing financial interests or personal relationships that could have appeared to influence the work reported in this paper.

Acknowledgement

The authors would like to thanks "Polısh Natıonal Agency For Academıc Exchange (NAWA) No. PPN/ULM/2020/1/00121" and National Science Centre (NCN) Project No. UMO-2020/37/K/ST8/02795 for financial supports. This work was also supported by the National Centre of Science (Decision No. 2017/25/B/ST8/00962).

Appendix A

Exp. No.	Cutting speed, v_c (m/min)	Feed, f (mm/rev)	Cooling Conditions
1	100	0,1	dry
2	150	0,1	dry
3	100	0,2	dry
4	150	0,2	dry
5	100	0,1	LN2
6	150	0,1	LN2
7	100	0,2	LN2
8	150	0,2	LN2
9	100	0,1	CO2
10	150	0,1	CO2
11	100	0,2	CO2
12	150	0,2	CO2

References

[1] H.A. Al-Tameemi, T. Al-Dulaimi, M.O. Awe, S. Sharma, D.Y. Pimenov, U. Koklu, K. Giasin, Evaluation of cutting-tool coating on the surface roughness and hole dimensional tolerances during drilling of Al6061-T651 alloy, Mater. 14 (2021), https://doi.org/10.3390/ma14071783.

[2] M. Sánchez-Carrilero, J.M. Sánchez-Sola, J.M. González, J.P. Contreras, M. Marcos, Cutting forces compatibility based on a plasticity model.: application to the oblique cutting of the AA2024 alloy, Int. J. Mach. Tools Manuf 42 (5) (2002) 559–565, https://doi.org/10.1016/S0890-6955(01)00157-2.

[3] G. List, M. Nouari, D. Géhin, S. Gomez, J.P. Manaud, Y. Le Petitcorps, F. Girot, Wear behaviour of cemented carbide tools in dry machining of aluminium alloy, Wear 259 (7-12) (2005) 1177–1189, https://doi.org/10.1016/j.wear.2005.02.056.

[4] H.-S. Kim, J. Chen, H.B. Lee, J.H. Shin, B.S. Kong, S. Oh, H. Jang, C. Jang, Effect of heat treatment on grain boundary carbides and primary water stress corrosion cracking resistance of Alloy 182 weld, Corros. Sci. (2021) 109730, https://doi.org/10.1016/j.corsci.2021.109730.

[5] Q. Sun, X. Liu, Q. Han, J. Li, R. Xu, K. Zhao, A comparison of AA2024 and AA7150 subjected to ultrasonic shot peening: microstructure, surface segregation and corrosion, Surf. Coatings Technol. 337 (2018) 552–560, https://doi.org/10.1016/j.surfcoat.2018.01.072.

[6] A. Iqbal, H. Suhaimi, W. Zhao, M. Jamil, M.M. Nauman, N. He, J. Zaini, Sustainable milling of Ti-6Al-4V: investigating the effects of milling orientation, cutter's helix angle, and type of cryogenic coolant, Metals (Basel). 10 (2020), https://doi.org/10.3390/met10020258.

[7] M. Kurt, Y. Kaynak, E. Bagci, Evaluation of drilled hole quality in Al 2024 alloy, Int. J. Adv. Manuf. Technol. 37 (2008) 1051–1060, https://doi.org/10.1007/s00170-007-1049-1.

[8] A.T. Abbas, D.Y. Pimenov, I.N. Erdakov, M.A. Taha, M.M. El Rayes, M.S. Soliman, Artificial intelligence monitoring of hardening methods and cutting conditions and their effects on surface roughness, performance, and finish turning costs of solid-state recycled aluminum alloy 6061 chips, Met. 8 (2018), https://doi.org/10.3390/met8060394.

[9] A. Shokrani, V. Dhokia, S.T. Newman, Environmentally conscious machining of difficult-to-machine materials with regard to cutting fluids, Int. J. Mach. Tools Manuf. 57 (2012) 83–101, https://doi.org/10.1016/j.ijmachtools.2012.02.002.

[10] S. Sun, M. Brandt, M.S. Dargusch, Thermally enhanced machining of hard-to-machine materials—a review, Int. J. Mach. Tools Manuf 50 (8) (2010) 663–680, https://doi.org/10.1016/j.ijmachtools.2010.04.008.

[11] M.S. Carrilero, R. Bienvenido, J.M. Sánchez, M. Álvarez, A. González, M. Marcos, A SEM and EDS insight into the BUL and BUE differences in the turning processes of AA2024 Al–Cu alloy, Int. J. Mach. Tools Manuf. 42 (2) (2002) 215–220, https://doi.org/10.1016/S0890-6955(01)00112-2.

[12] I. Puertas Arbizu, C.J. Luis Pérez, Surface roughness prediction by factorial design of experiments in turning processes, J. Mater. Process. Technol. 143–144 (2003) 390–396, https://doi.org/10.1016/S0924-0136(03)00407-2.

[13] M. Nouari, G. List, F. Girot, D. Géhin, Effect of machining parameters and coating on wear mechanisms in dry drilling of aluminium alloys, Int. J. Mach. Tools Manuf. 45 (12-13) (2005) 1436–1442, https://doi.org/10.1016/j.ijmachtools.2005.01.026.

[14] M. Danish, T. Ginta, B.A. Wahjoedi, Enhanced functional properties of Mg alloys by cryogenic machining, Int. J. Appl. Eng. Res. 11 (2016) 5055–5059.

[15] N.S. Kalsi, R. Sehgal, V.S. Sharma, Cryogenic treatment of tool materials: a review, Mater. Manuf. Process. 25 (10) (2010) 1077–1100, https://doi.org/10.1080/10426911003720862.

[16] M. Danish, T.L. Ginta, K. Habib, A.M. Abdul Rani, B.B. Saha, Effect of cryogenic cooling on the heat transfer during turning of AZ31C magnesium alloy, Heat Transf. Eng. 40 (12) (2019) 1023–1032, https://doi.org/10.1080/01457632.2018.1450345.

[17] M. Dogra, V.S. Sharma, A. Sachdeva, N.M. Suri, J.S. Dureja, Performance evaluation of CBN, coated carbide, cryogenically treated uncoated/coated carbide inserts in finish-turning of hardened steel, Int. J. Adv. Manuf. Technol. 57 (5-8) (2011) 541–553, https://doi.org/10.1007/s00170-011-3320-8.

[18] M. Danish, T.L. Ginta, A.M. Abdul Rani, D. Carou, J.P. Davim, S. Rubaiee, S. Ghazali, Investigation of surface integrity induced on AZ31C magnesium alloy turned under cryogenic and dry conditions, Procedia Manuf. 41 (2019) 476–483, https://doi.org/10.1016/j.promfg.2019.09.035.

[19] N.S. Kalsi, R. Sehgal, V.S. Sharma, Effect of tempering after cryogenic treatment of tungsten carbide-cobalt bounded inserts, Bull. Mater. Sci. 37 (2) (2014) 327–335, https://doi.org/10.1007/s12034-014-0634-9.
[20] C. Agrawal, J. Wadhwa, A. Pitroda, C.I. Pruncu, M. Sarikaya, N. Khanna, Comprehensive analysis of tool wear, tool life, surface roughness, costing and carbon emissions in turning Ti–6Al–4V titanium alloy: Cryogenic versus wet machining, Tribol. Int. 153 (2021) 106597, https://doi.org/10.1016/j.triboint.2020.106597.
[21] S.Y. Hong, Y. Ding, Micro-temperature manipulation in cryogenic machining of low carbon steel, J. Mater. Process. Technol. 116 (1) (2001) 22–30, https://doi.org/10.1016/S0924-0136(01)00836-6.
[22] P. Sivaiah, D. Chakradhar, Performance improvement of cryogenic turning process during machining of 17–4 PH stainless steel using multi objective optimization techniques, Measurement 136 (2019) 326–336, https://doi.org/10.1016/j.measurement.2018.12.094.
[23] M. Jebaraj, M. Pradeep Kumar, R. Anburaj, Effect of LN2 and CO2 coolants in milling of 55NiCrMoV7 steel, J. Manuf. Process. 53 (2020) 318–327, https://doi.org/10.1016/j.jmapro.2020.02.040.
[24] N. Khanna, P. Shah, Chetan, Comparative analysis of dry, flood, MQL and cryogenic CO2 techniques during the machining of 15–5-PH SS alloy, Tribol. Int. 146 (2020) 106196, https://doi.org/10.1016/j.triboint.2020.106196.
[25] J.C. Outeiro, F. Rossi, G. Fromentin, G. Poulachon, G. Germain, A.C. Batista, Process mechanics and surface integrity induced by dry and cryogenic machining of AZ31B-O magnesium alloy, Procedia CIRP. 8 (2013) 487–492, https://doi.org/10.1016/j.procir.2013.06.138.
[26] Y. Kaynak, Evaluation of machining performance in cryogenic machining of Inconel 718 and comparison with dry and MQL machining, Int. J. Adv. Manuf. Technol. 72 (5-8) (2014) 919–933, https://doi.org/10.1007/s00170-014-5683-0.
[27] J. Eapen, S. Murugappan, S. Arul, A study on chip morphology of aluminum alloy 6063 during turning under pre cooled cryogenic and dry environments, Mater. Today:. Proc. 4 (8) (2017) 7686–7693, https://doi.org/10.1016/j.matpr.2017.07.103.
[28] D.Y. Pimenov, V.I. Guzeev, Mathematical model of plowing forces to account for flank wear using FME modeling for orthogonal cutting scheme, Int. J. Adv. Manuf. Technol. 89 (9-12) (2017) 3149–3159, https://doi.org/10.1007/s00170-016-9216-x.
[29] S. Li, J. Sui, F. Ding, S. Wu, W. Chen, C. Wang, Optimization of milling aluminum alloy 6061–T6 using modified Johnson-cook model, Simul. Model. Pract. Theory 111 (2021) 102330, https://doi.org/10.1016/j.simpat.2021.102330.
[30] R.A. Mali, M.D. Agrahari, T.V.K. Gupta, FE based simulation and experimental validation of forces in dry turning of aluminium 7075, Mater. Today:. Proc. 27 (2020) 2319–2323, https://doi.org/10.1016/j.matpr.2019.09.120.
[31] H.V. Lima, A.F.V. Campidelli, A.A.T. Maia, A.M. Abrão, Temperature assessment when milling AISI D2 cold work die steel using tool-chip thermocouple, implanted thermocouple and finite element simulation, Appl. Therm. Eng. 143 (2018) 532–541, https://doi.org/10.1016/j.applthermaleng.2018.07.107.
[32] M. Baraheni, A. Bagheri Bami, A. Alaei, S. Amini, Ultrasonic-assisted friction drilling process of aerospace aluminum alloy (AA7075): FEA and experimental study, Int. J. Light. Mater. Manuf. 4 (2021) 315–322, https://doi.org/10.1016/j.ijlmm.2021.03.001.
[33] M. Khajehzadeh, O. Boostanipour, M. Reza Razfar, Finite element simulation and experimental investigation of residual stresses in ultrasonic assisted turning, Ultrasonics 108 (2020) 106208, https://doi.org/10.1016/j.ultras.2020.106208.
[34] X. Huang, J. Xu, M. Chen, F. Ren, Finite element modeling of high-speed milling 7050–T7451 alloys, Procedia Manuf. 43 (2020) 471–478, https://doi.org/10.1016/j.promfg.2020.02.186.
[35] J.-H. Urrea-Quintero, M. Marino, H. Hernandez, S. Ochoa, Multiscale modeling of a free-radical emulsion polymerization process: numerical approximation by the Finite Element Method, Comput. Chem. Eng. 140 (2020) 106974, https://doi.org/10.1016/j.compchemeng.2020.106974.
[36] K.O. Coelho, P.R.B. Devloo, S.M. Gomes, Error estimates for the Scaled Boundary Finite Element Method, Comput. Methods Appl. Mech. Eng. 379 (2021) 113765, https://doi.org/10.1016/j.cma.2021.113765.
[37] N. Yaşar, Thrust force modelling and surface roughness optimization in drilling of AA-7075: FEM and GRA, J. Mech. Sci. Technol. 33 (10) (2019) 4771–4781, https://doi.org/10.1007/s12206-019-0918-5.
[38] K. Gok, Development of three-dimensional finite element model to calculate the turning processing parameters in turning operations, Measurement 75 (2015) 57–68, https://doi.org/10.1016/J.MEASUREMENT.2015.07.034.
[39] S. Savidis, D. Aubram, F. Rackwitz, Arbitrary Lagrangian-Eulerian finite element formulation for geotechnical construction processes, J. Theor. Appl. Mech. 38 (2008) 165–194.
[40] W. Grzesik, Chapter Nine – Heat in Metal Cutting, in: W.B.T.-A.M.P. of M.M. Grzesik (Eds.)), Adv. Mach. Process. Met. Mater., second ed., Elsevier, 2017, pp. 163–182. https://doi.org/10.1016/B978-0-444-63711-6.00009-0.
[41] F. Jafarian, M. Imaz Ciaran, D. Umbrello, P.J. Arrazola, L. Filice, H. Amirabadi, Finite element simulation of machining Inconel 718 alloy including microstructure changes, Int. J. Mech. Sci. 88 (2014) 110–121, https://doi.org/10.1016/j.ijmecsci.2014.08.007.
[42] S.K. Mishra, S. Ghosh, S. Aravindan, 3D finite element investigations on textured tools with different geometrical shapes for dry machining of titanium alloys, Int. J. Mech. Sci. 141 (2018) 424–449, https://doi.org/10.1016/j.ijmecsci.2018.04.011.
[43] M.E. Korkmaz, P. Verleysen, M. Günay, Identification of constitutive model parameters for nimonic 80A superalloy, Trans. Indian Inst. Met. 71 (12) (2018) 2945–2952, https://doi.org/10.1007/s12666-018-1394-9.
[44] M.E. Korkmaz, M. Günay, P. Verleysen, Investigation of tensile Johnson-Cook model parameters for Nimonic 80A superalloy, J. Alloys Compd. 801 (2019) 542–549, https://doi.org/10.1016/J.JALLCOM.2019.06.153.
[45] X. Xu, J. Zhang, J. Outeiro, B. Xu, W. Zhao, Multiscale simulation of grain refinement induced by dynamic recrystallization of Ti6Al4V alloy during high speed machining, J. Mater. Process. Technol. 286 (2020) 116834, https://doi.org/10.1016/j.jmatprotec.2020.116834.
[46] X. Xie, G. Kang, Q. Kan, C. Yu, Phase-field theory based finite element simulation on thermo-mechanical cyclic deformation of polycrystalline super-elastic NiTi shape memory alloy, Comput. Mater. Sci. 184 (2020) 109899, https://doi.org/10.1016/j.commatsci.2020.109899.
[47] M.E. Korkmaz, N. Yaşar, M. Günay, Numerical and experimental investigation of cutting forces in turning of Nimonic 80A superalloy, Eng. Sci. Technol. an Int. J. 23 (3) (2020) 664–673, https://doi.org/10.1016/j.jestch.2020.02.001.
[48] S.K. Josyula, S.K.R. Narala, Study of TiC particle distribution in Al-MMCs using finite element modeling, Int. J. Mech. Sci. 141 (2018) 341–358, https://doi.org/10.1016/j.ijmecsci.2018.04.004.
[49] B. Haddag, S. Atlati, M. Nouari, A. Moufki, Dry machining aeronautical aluminum alloy AA2024-T351: analysis of cutting forces, chip segmentation and built-up edge formation, Met. 6 (2016), https://doi.org/10.3390/met6090197.
[50] S. Canovic, B. Ljungberg, C. Björmander, M. Halvarsson, CVD TiC/alumina and TiN/alumina multilayer coatings grown on sapphire single crystals, Int. J. Refract Metal Hard Mater. 28 (2) (2010) 163–173, https://doi.org/10.1016/j.ijrmhm.2009.08.001.
[51] M. Du, Z. Cheng, S. Wang, Finite element modeling of friction at the tool-chip-workpiece interface in high speed machining of Ti6Al4V, Int. J. Mech. Sci. 163 (2019) 105100, https://doi.org/10.1016/j.ijmecsci.2019.105100.
[52] M. Akgün, H. Demir, Optimization of cutting parameters affecting surface roughness in turning of inconel 625 superalloy by cryogenically treated tungsten carbide inserts, SN Appl. Sci. 3 (2021) 277, https://doi.org/10.1007/s42452-021-04303-2.
[53] H. Kaya, O. Uluer, E. Kocaoğlu, V. Kirmaci, Experimental analysis of cooling and heating performance of serial and parallel connected counter-flow Ranquee-Hilsch vortex tube systems using carbon dioxide as a working fluid, Int. J. Refrig. 106 (2019) 297–307, https://doi.org/10.1016/j.ijrefrig.2019.07.004.
[54] M.K. Gupta, Q. Song, Z. Liu, M. Sarikaya, M. Mia, M. Jamil, A.K. Singla, A. Bansal, D.Y. Pimenov, M. Kuntoğlu, Tribological performance based machinability investigations in cryogenic cooling assisted turning of α-β titanium Alloy, Tribol. Int. 160 (2021) 107032, https://doi.org/10.1016/j.triboint.2021.107032.
[55] Y.M. Arisoy, C. Guo, B. Kaftanoğlu, T. Özel, Investigations on microstructural changes in machining of Inconel 100 alloy using face turning experiments and 3D finite element simulations, Int. J. Mech. Sci. 107 (2016) 80–92, https://doi.org/10.1016/j.ijmecsci.2016.01.009.
[56] Y. Yang, L. Jin, J. Zhu, J. Kong, L. Li, Study on cutting force, cutting temperature and machining residual stress in precision turning of pure iron with different grain sizes, Chin. J. Mech. Eng. 33 (2020) 53, https://doi.org/10.1186/s10033-020-00471-1.
[57] B.N. Pathak, K.L. Sahoo, M. Mishra, Effect of machining parameters on cutting forces and surface roughness in Al-(1–2) Fe-1V-1Si alloys, Mater. Manuf. Process. 28 (4) (2013) 463–469, https://doi.org/10.1080/10426914.2013.763952.
[58] U. Şeker, A. Kurt, İ. Çiftçi, The effect of feed rate on the cutting forces when machining with linear motion, J. Mater. Process. Technol. 146 (3) (2004) 403–407, https://doi.org/10.1016/j.jmatprotec.2003.12.001.
[59] M.A.P. Juárez, E.A. Gómez, H. Plascencia-Mora, E.L. Orozco, J.F.R. Arredondo, M. L.C. Silva, Finite element simulation and experimental analysis of cutting forces in orthogonal turning in AISI-1045 steel, Comput. y Sist. 23 (2019) 7.
[60] J. Hou, W. Zhou, H. Duan, G. Yang, H. Xu, N. Zhao, Influence of cutting speed on cutting force, flank temperature, and tool wear in end milling of Ti-6Al-4V alloy, Int. J. Adv. Manuf. Technol. 70 (9-12) (2014) 1835–1845, https://doi.org/10.1007/s00170-013-5433-8.
[61] Q. Shi, L. Li, N. He, W. Zhao, X. Liu, Experimental study in high speed milling of titanium alloy TC21, Int. J. Adv. Manuf. Technol. 64 (1-4) (2013) 49–54, https://doi.org/10.1007/s00170-012-3997-3.
[62] P.R. Paresi, Y. Lou, A. Narayanan, J.W. Yoon, Enhanced constitutive model for aeronautic aluminium alloy (AA2024-T351) under high strain rates and elevated temperatures, Int. J. Automot. Technol. 20 (S1) (2019) 79–87, https://doi.org/10.1007/s12239-019-0130-8.
[63] S. Ravi, M. Pradeep Kumar, Experimental investigations on cryogenic cooling by liquid nitrogen in the end milling of hardened steel, Cryogenics (Guildf) 51 (9) (2011) 509–515, https://doi.org/10.1016/j.cryogenics.2011.06.006.
[64] F. Pusavec, A. Deshpande, S. Yang, R. M'Saoubi, J. Kopac, O.W. Dillon, I. S. Jawahir, Sustainable machining of high temperature Nickel alloy – inconel 718: part 1 – predictive performance models, J. Clean. Prod. 81 (2014) 255–269, https://doi.org/10.1016/j.jclepro.2014.06.040.
[65] S.Y. Hong, Y. Ding, W. Cheol Jeong, Friction and cutting forces in cryogenic machining of Ti-6Al-4V, Int. J. Mach. Tools Manuf. (2001), https://doi.org/10.1016/S0890-6955(01)00029-3.
[66] P. Singh, H. Pungotra, N.S. Kalsi, On the complexities in machining titanium alloys, in: D.K. Mandal, C.S. Syan (Eds.), CAD/CAM, Robot. Factories Futur., Springer India, New Delhi, 2016, pp. 499–507.
[67] A. Pramanik, Problems and solutions in machining of titanium alloys, Int. J. Adv. Manuf. Technol. 70 (5-8) (2014) 919–928, https://doi.org/10.1007/s00170-013-5326-x.
[68] Kiprawi, Mohammad Ashaari, Yassin, Abdullah, Syed Shazali, Syed Tarmizi, Islam, M. Shahidul, Mohd Said, Mohd Azrin, Study of cutting edge temperature and

cutting force of end mill tool in high speed machining, in: MATEC Web Conf. vol. 87, 2017, pp. 2030. https://doi.org/10.1051/matecconf/20178702030.
[69] J. Hua, R. Shivpuri, X. Cheng, V. Bedekar, Y. Matsumoto, F. Hashimoto, T. R. Watkins, Effect of feed rate, workpiece hardness and cutting edge on subsurface residual stress in the hard turning of bearing steel using chamfer+hone cutting edge geometry, Mater. Sci. Eng., A 394 (1-2) (2005) 238–248, https://doi.org/10.1016/j.msea.2004.11.011.
[70] H.-B. He, H.-Y. Li, J. Yang, X.-Y. Zhang, Q.-B. Yue, X. Jiang, S.-ki. Lyu, A study on major factors influencing dry cutting temperature of AISI 304 stainless steel, Int. J. Precis. Eng. Manuf. 18 (10) (2017) 1387–1392, https://doi.org/10.1007/s12541-017-0165-6.
[71] M. Danish, T.L. Ginta, K. Habib, D. Carou, A.M.A. Rani, B.B. Saha, Thermal analysis during turning of AZ31 magnesium alloy under dry and cryogenic conditions, Int. J. Adv. Manuf. Technol. 91 (5-8) (2017) 2855–2868, https://doi.org/10.1007/s00170-016-9893-5.
[72] T. Özel, M. Sima, A.K. Srivastava, B. Kaftanoglu, Investigations on the effects of multi-layered coated inserts in machining Ti–6Al–4V alloy with experiments and finite element simulations, CIRP Ann. 59 (1) (2010) 77–82, https://doi.org/10.1016/j.cirp.2010.03.055.
[73] T. Özel, D. Ulutan, Prediction of machining induced residual stresses in turning of titanium and nickel based alloys with experiments and finite element simulations, CIRP Ann. 61 (1) (2012) 547–550, https://doi.org/10.1016/j.cirp.2012.03.100.
[74] Y. Guo, G. Quan, M. Celikin, L. Ren, Y. Zhan, L. Fan, H. Pan, Effect of heat treatment on the microstructure and mechanical properties of AZ80M magnesium alloy fabricated by wire arc additive manufacturing, J. Magnes. Alloy. (2021), https://doi.org/10.1016/j.jma.2021.04.006.
[75] L. Li, M. Mahmoodian, C.-Q. Li, D. Robert, Effect of corrosion and hydrogen embrittlement on microstructure and mechanical properties of mild steel, Constr. Build. Mater. 170 (2018) 78–90, https://doi.org/10.1016/j.conbuildmat.2018.03.023.
[76] L. Wang, S. Jia, Y. Yi, G. Liu, L. Sun, L. Shi, S. Ma, Effects of damage evolution on tensile strength measurement of nuclear graphite material by ring compression test, J. Nucl. Mater. 555 (2021) 153128, https://doi.org/10.1016/j.jnucmat.2021.153128.
[77] Q. Zheng, T. Furushima, Evaluation of high-temperature tensile behavior for metal foils by a novel resistance heating assisted tensile testing system using samples with optimized structures, J. Mater. Sci. Technol. 94 (2021) 216–229, https://doi.org/10.1016/j.jmst.2021.03.061.
[78] M. Abdel-Salam, S. El-Hadad, W. Khalifa, Effects of microstructure and alloy composition on hydroxyapatite precipitation on alkaline treated α/β titanium alloys, Mater. Sci. Eng., C 104 (2019) 109974, https://doi.org/10.1016/j.msec.2019.109974.
[79] B. Fu, H. Wang, C. Zou, Z. Wei, The influence of Zr content on microstructure and precipitation of silicide in as-cast near α titanium alloys, Mater. Charact. 99 (2015) 17–24, https://doi.org/10.1016/j.matchar.2014.09.015.
[80] S. Schindler, M. Zimmermann, J.C. Aurich, P. Steinmann, Thermo-elastic deformations of the workpiece when dry turning aluminum alloys - A finite element model to predict thermal effects in the workpiece, CIRP J. Manuf. Sci. Technol. 7 (3) (2014) 233–245, https://doi.org/10.1016/j.cirpj.2014.04.006.
[81] C. Wang, H. Ding, H. Wang, Thermodynamic model and dynamic temperature compensation in positive-pressure-based sonic nozzle gas flow standard, IEEE Trans. Instrum. Meas. 62 (5) (2013) 1154–1165, https://doi.org/10.1109/TIM.2012.2234599.
[82] R. Zimmerschied, R. Isermann, Nonlinear time constant estimation and dynamic compensation of temperature sensors, Control Eng. Pract. – Control ENG Pract. 18 (3) (2010) 300–310, https://doi.org/10.1016/j.conengprac.2009.11.008.